Available online at www.sciencedirect.com
ScienceDirect
Journal of Power Sources 164 (2007) 839–848
JOURNAL OF POWER SOURCES
www.elsevier.com/locate/jpowsour

Structure, texture and reactivity versus lithium of chromium-based oxides films as revealed by TEM investigations

L. Dupont *, S. Grugeon, S. Laruelle, J-M. Tarascon

LRCS-UMR 6007, Université de Picardie Jules Verne, 33 Rue Saint-Leu, 80039 Amiens, France

Received 7 July 2006; received in revised form 20 September 2006; accepted 24 October 2006
Available online 8 December 2006

Abstract

Analytical high resolution transmission electron microscopy has been used to clearly evidence the electrochemical reactivity of Cr_2O_3 thin films versus lithium. We showed that during the reduction process, chromium sesquioxide (+III) transforms first into chromium monoxide (+II) and then into metallic chromium nanoparticles embedded into a Li_2O matrix at 0 V. On the subsequent recharge up to 3 V, we did not convert back to Cr_2O_3, but only to a chromium monoxide implying a partial re-oxidation process, thus explaining the irreversibility measured during the first cycle. We extended this study to the comprehension of the electrochemical performances of Cr_2O_3-based electrodes obtained by thermal treatment, under different atmospheres, of chromium rich stainless steel disks. In addition to the characterization of the particles forming the so-obtained electro-active layers, we showed, using nano-probe EDS, that a mixed "Fe–Cr–O" oxide could react versus lithium, through a conversion reaction mechanism, leading to alloyed metallic nanoparticles upon reduction and nanograins of mixed oxide during the following oxidation.

Keywords: Transmission electron microscopy; Lithium-ion battery; Chromium oxide; Conversion reaction; Stainless steel

1. Introduction

Nowadays, rechargeable Li-ion batteries operate through intercalation reactions limited to the insertion of one lithium per 3d-metal. Seeking for better electrodes, a few research teams have explored new routes leading to promising results [1–3]. For instance, our group reported a Li-electrochemically driven CoO/Co conversion process involving a $2e^-$ reversible charge transfer per 3d-metal [4–10] leading to outstanding capacity gains. Therefore the redox potential (1.7 V) at which this reaction occurs is unsuitable for positive or negative electrodes applications. The potential of such conversion reactions being governed by the iono-covalency of the M–O bonding, we could deduce from simple calculations [11] that, potential-wise, the most interesting oxide to be used as negative electrode material would be Cr_2O_3. Unfortunately, the poor electronic conductivity of this oxide makes its utilization difficult. To solve this problem, one possibility proposed By Hu [12] is the formation of Cr_2O_3/carbon composites within which Cr_2O_3 particles are coated with a thin layer of carbon. Using such an approach the authors have drastically enhanced the capacity retention of Cr_2O_3-based electrodes however to the expense of an initial capacity loss owing to the large amounts of carbon used. Another conceivable strategy, as pursued by our group, consists in designing electrode configuration to enhance the contact between the current collector and the oxide. Along that approach, two strategies were developed. The first one consisted in the growth of chromium oxide thin films by pulsed laser deposition technique with the end result being the feasibility of using conversion reactions without any carbon additives if the film thickness is lower than 175 nm. In the second approach, we took advantage of the stainless steel corrosion properties so as to favour the growth of a chromium rich oxide layer, through appropriate thermal treatments under different atmospheres, having outstanding capacity retention [13].

The X-ray diffraction analysis of these electrodes revealed the coexistence of two chromium-rich oxide phases: a chromite phase having the spinel structure and a sesquioxide-type phase having the corundum structure. In order to have more information on the morphology, structure and composition at the atomic scale of the pristine and cycled oxide particles, we undertook an analytical high resolution transmission electron microscopy

* Corresponding author. Tel.: +33 3 22 82 75 85; fax: +33 3 22 82 75 90.
E-mail address: loic.dupont@sc.u-picardie.fr (L. Dupont).

0378-7753/$ – see front matter © 2006 Elsevier B.V. All rights reserved.
doi:10.1016/j.jpowsour.2006.10.096

study using a TECNAI F20 microscope fitted with EDS analysis. For reasons of clarity, we will first report the results obtained on PLD grown Cr_2O_3 thin films, which will act as a reference throughout this study. Then, the results on stainless steel, especially the effect of parameters such as atmosphere and annealing temperature on the composition of the surface oxides, will be presented; the main highlight is the feasibility to reversibly form an alloy from a mixed binary oxide ($M_{1-x}M'_x$–O) phase.

2. Experimental

2.1. PLD Cr_2O_3 thin film samples

Chromium oxide Cr_2O_3 thin films were deposited on a 1.37 cm^2 Ti substrate by Pulsed laser Deposition (PLD), using KrF excimer laser beam (Lambda physik, Compex 102, $\lambda = 248$ nm) with a laser fluency of 2 J cm^{-2}. A Cr pellet was used as the target with a 4 cm target–substrate distance. The pressure in the chamber was fixed at 5×10^{-2} mbar of oxygen. The substrate temperature was altered from 25 to 400 °C, and we used a laser-shooting repetition rate of 10 Hz for times running from about 10 min to 6 h. Using such conditions, films with thicknesses running from about 40 nm to about 500 nm, as determined by means of a profilometer, were obtained.

2.2. Stainless steel samples

Experiments were conducted using 1.88 cm^2 stainless steel disks (SUS316L). This stainless steel is made of 70% iron, 17–19% chromium, 12.5–15% Ni, 2–3% Mo, 1–2% Mn, 0.5–1% Si and traces of other elements such as P, S, and N. The disks were heated at 5 °C min^{-1} up to 700 or 800 °C under various atmospheres, and were maintained for 13 h at this temperature prior to being cooled down. The gas used were argon, nitrogen (impurities: O_2, H_2O 2 vpm), a mixture of 10% hydrogen in nitrogen (O_2, H_2O 5 vpm) and air.

2.3. Electrochemical tests

Electrochemical tests versus lithium were performed using coin cells (standard 2035-size) that were assembled in an argon filled dry-box. Studied sample was separated from a lithium disk used as the negative electrode by a borosilicate micro-fibre (Millipore) film impregnated with 0.5 ml of a $LiPF_6$ (1 M) in EC–DMC (1–1) solution. The electrochemical tests were carried out using a VMP system (Biologic S.A., Claix, France) that can be operated in both potentiodynamic and galvanostatic modes at 55 °C in the 0.02–3 V potential window. All reported potential values are given versus Li/Li^+.

2.4. Analytical high resolution transmission electron microscopy

Transmission electron microscopy was carried out using a FEI TECNAI F20 ST microscope, equipped with both energy dispersive spectroscopy (EDS) analysis capabilities and a home designed sample holder for moisture sensitive samples. Samples were prepared by scratching the surface with a diamond tip; the resulting chips being transferred to the Copper TEM holey carbon grid through a drop of alcohol deposited on the disk surface. Recorded SAED patterns were converted in equivalent XRD pattern (Cu Kα radiation) using the process diffraction software [14] in order to determine the implied phases.

3. Results and discussion

3.1. PLD Cr_2O_3 thin films

Irrespective of the thicknesses, chromium oxide thin films deposited at room temperature are formed of 1 to 20 nm amorphous grains. At 400 °C larger grains, which size exceeds 50 nm for some of them, are observed (Fig. 1a). The indexing of their corresponding powder SAED patterns (inset Fig. 1a), by means of process diffraction software (Fig. 1b), unambiguously evidences an Eskolaite phase (Cr_2O_3), whereas high resolution image (Fig. 1c) realized along the $[12–1]^*$ zone axis (inset Fig. 1c) reveals very well crystallized crystallites.

Fig. 2a shows the potential/composition curve obtained from the galvanostatic cycling of a room temperature PLD deposited Cr_2O_3 film/Li cell performed at a nominal C rate ($1Li^+ h^{-1}$) in the 0.05–3.0 V potential window. The first discharge process is characterized by the appearance of two plateaus located at 0.4 and 0.2 V with an overall uptake of 6 Li. Upon subsequent charge, the voltage increases smoothly and continuously from 0.02 to 3 V with an overall release of 4 Li implying a 33% irreversible capacity with therefore an overall reversible capacity of 750 mAh g^{-1}. Such results do not come as a surprise, but simply suggest a classical conversion reaction process with the reduction of Cr^{3+} in Cr^0 and its re-oxidation in Cr^{2+}. To confirm such a statement and to understand the origin of the 0.4 V plateau, partially and fully reduced as well as re-oxidized films were investigated by high-resolution transmission electron microscopy.

The PLD films, discharged to a potential of 0.35 V (namely after the first plateau), are badly crystallized (Fig. 2 b). Only broad rings are present on the SAED pattern. Nevertheless, the formation of a CrO phase ($a = 4.04$ Å, S.G.: *Fm*-3*m*) could be suggested to successfully index the process diffraction diagram (right inset) and the FFT (left inset) taken on one of the few 3 nm nanoparticles lying along the c^* axis. Such a proposition is consistent with the electrochemical data since the material was shown to react with two lithium ions implying a reduction of the chromium ions from 3^+ to 2^+ degree. Along that line it is worth noting that in literature, chromium monoxide, which is a metastable phase, is reported with the $CrO_{0.87}$ composition (JCPDS 78–0722) whilst it is based on the same NaCl-type structure as other transition metal monoxides such as MnO or FeO. For convenience reasons, from now on in the text the $CrO_{0.87}$ phase will be referred to as CrO.

When the Cr_2O_3 film is fully reduced (Fig. 2c), the bright field image reveals the presence of 2–3 nm Cr nanoparticles embedded into a Li_2O matrix (as deduced from the SAED patterns). Upon the following charge (3.0 V), the SAED pattern (Fig. 2d) clearly shows the vanishing of the Cr and Li_2O reflections at the

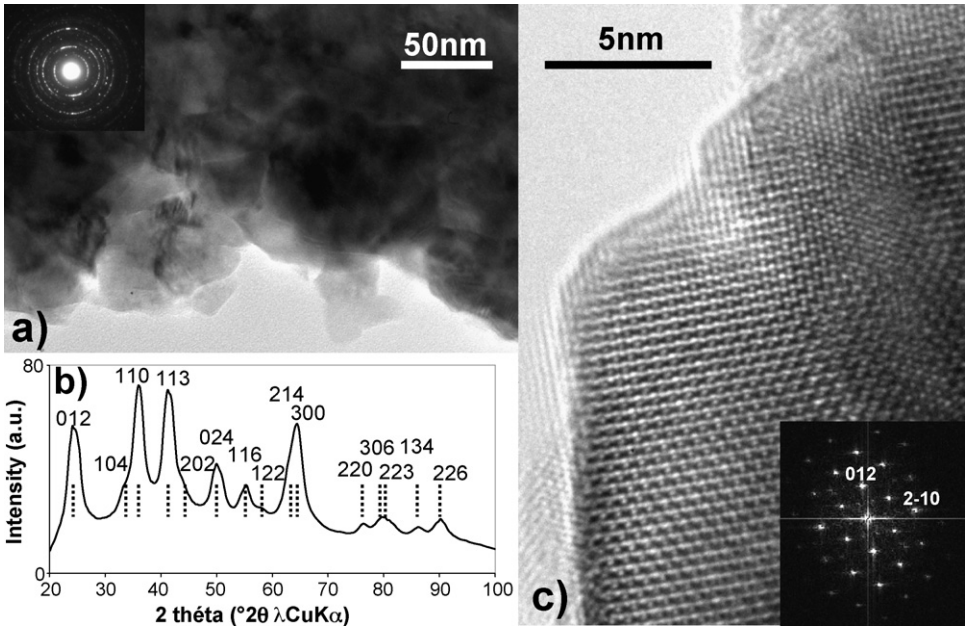

Fig. 1. TEM study of the post-annealed Cr_2O_3 film at 400 °C. (a) Bright field image together with corresponding SAED pattern (inset). (b) Indexing of the XRD like diagram obtained by treatment of the SAED pattern. (c) High resolution image together with the FFT (inset).

expense of those of the CrO phase, thus confirming the classical reported conversion mechanism.

Regarding the cycling behaviour, we experienced that the best capacity retention was obtained for Cr_2O_3 films thinner than 200 nm. For higher thicknesses, rapid capacity decays, most likely due to the loss of electronic percolating path within the electrode, were noted upon cycling. Whatever the origin of this capacity fading, these results demonstrate that the use of reversible conversion reactions without any carbon additives in lithium batteries is possible only if the thickness of the active material is not too large. As the PLD technique limits the sample size, the retained solution to prepare electrodes having large Cr_2O_3-covered surfaces consisted in using high surface Cr-based stainless steel current collector as substrates for the

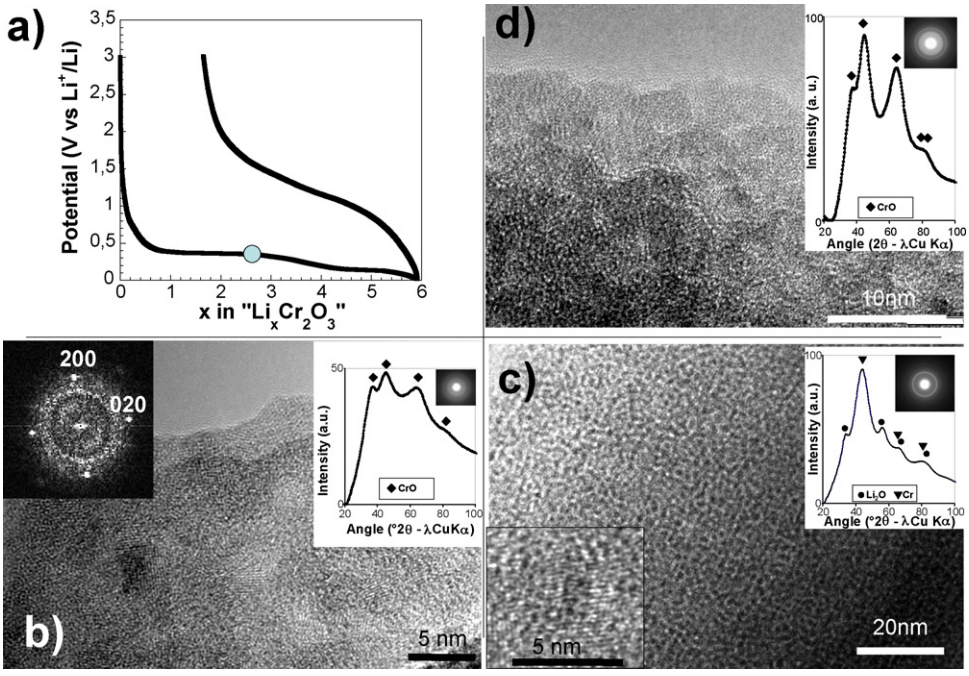

Fig. 2. (a) Voltage–composition trace for an ablated Cr_2O_3/Li cell cycled between 0.02 and 3 V. The dot denotes the cut-off voltage for the partially discharged material. (b) TEM image realized on the partially discharged material showing CrO nanoparticles. (c) TEM image on a fully reduced ablated electrode showing crystallized chromium nanoparticles (enlarged image of one of them is given, bottom inset) embedded in Li_2O as deduced from the processed SAED pattern given in the top inset. (d) TEM image realized on the re-oxidized electrode up to 3 V showing partial re-oxidation into CrO nanoparticles as deduced by processed SAED pattern given in inset.

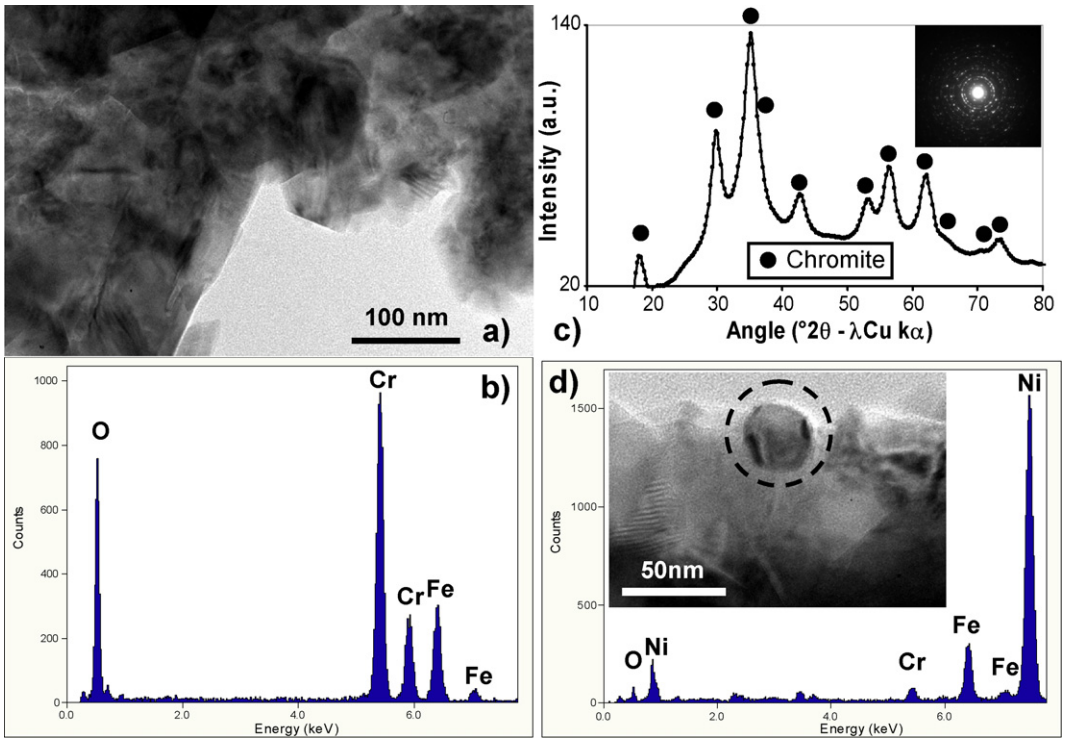

Fig. 3. (a) TEM image realized on a treated sample showing that the disk surface is made of aggregates and crystallites that can reach a coherence length as large as 100 nm. By combining the processed EDS analysis (b) and SAED pattern results (c), the nature of the matter forming the platelets is deduced to be a chromite phase whose formula can be written as $(Fe_xCr_{1-x})(Cr_2)O_4$. Besides the chromite-phase, metallic Ni/Fe nodules of 20–50 nm showing different shapes (d) could be identified.

growth of oxide layers through a high temperature treatment process.

3.2. Chromium rich stainless steel disks treatment

The precursor stainless steel material substrates were heated under various atmospheres (nitrogen with 10% hydrogen, pure nitrogen, argon or air) up to 700 or 800 °C (starting material characteristics and thermal treatment procedure are described in Section 2).

Representative TEM images realized on sample treated under nitrogen with 10% hydrogen at 700 °C evidence aggregates of platelet-shape crystals as large as 100 nm (Fig. 3a), which were shown by EDS to contain both Fe and Cr but not Ni (Fig. 3b). Besides, we note evidence for large amounts of oxygen suggesting that iron and chromium have most likely combined with oxygen to form oxides. The collected SAED patterns (Fig. 3c) show well-defined spotted rings that turned out to be characteristics of a chromite phase (JCPDS 34–0140), which formula can be written as (Fe_xCr_{1-x}) $(Cr_2)O_4$. Moreover, by further scrutinizing the treated sample surface, nodules of 20–50 nm showing different shapes have been identified (Fig. 3d), and were mainly composed of metallic Ni with tiny amounts of iron (almost no oxygen is detected). The origin of O, Cr and Fe peaks spotted on the EDS spectra is simply explained by the fact that the observed metallic Ni/Fe particle is lying onto a chromite particle so that some interferences do occur. Besides these Ni-rich particles, others made of Eskolaite phase (Cr_2O_3) were also observed. Overall, TEM studies strongly suggest that the thermal treatment promotes the formation of an oxide layer through a migration of the metallic elements resulting in an enrichment of the stainless steel surface in Cr content at the expense of depletion in Fe and Ni contents. Chromium oxide being one of the most stable oxides, the freshly migrated Cr atoms will react, at the surface, with traces of oxygen present within the reducing flowing gas to form the chromite phase. In light of these results, the effect of temperature and atmosphere on the nature and composition of the oxides was studied.

3.3. Effect of the various heating atmospheres

Experiments were realized at 700 °C using various gases, listed by decreasing reducing power, namely nitrogen with 10% hydrogen, pure nitrogen, argon and air noted N_2/H_2, N_2, Ar and R, respectively. Regardless of the gases used, all the samples contain two populations of particles. The bright field images recorded at low magnification for the N_2, Ar and R treated samples are shown in Fig. 4. On theses images, platelets whose size range from 100 nm to 1 μm and octahedra having sizes close to 200 nm wide (with a darkest contrast due to a larger thickness) are observed. From both EDS and electron diffraction studies, we could establish a direct relation between the particles shape and their structural-type phase composition. The platelets are made of pure Eskolaite phase (Cr_2O_3) while octahedra particles are made of $Mn_xFe_yCr_{3-z}O_4$ chromite-type phase (with $z = x + y$). The crystallinity of the Cr_2O_3 platelets is sensitive

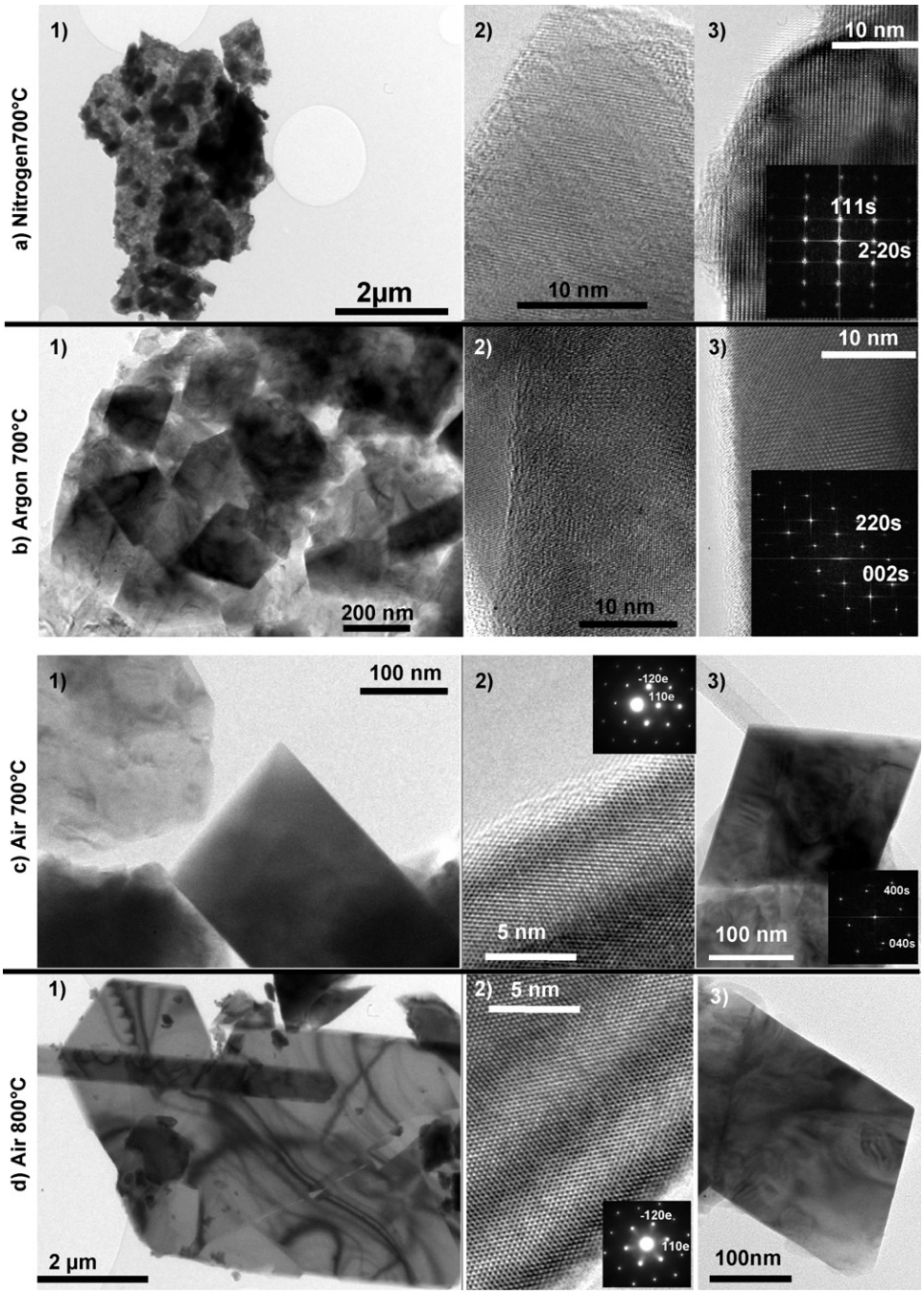

Fig. 4. TEM study realized on stainless steel treated at: (a) 700 °C under nitrogen, (b) 700 °C under argon, (c) 700 °C under air, 800 °C under air. Index 1: overall bright field image showing two populations of particles. Index 2: high resolution image realized on the platelets showing the crystallinity evolution and SAED pattern assigned to Cr_2O_3 phase are given in inset as soon as the material is crystallized, Index 3: bright field or high resolution images realized on the octahedron together with SAED pattern assigned to chromite-type phase.

to the nature of the used gas. High resolution images realized on eskolaite particles show poorly, badly and well crystallized contrasts (see index 2, Fig. 4) for samples treated under nitrogen, argon and air, respectively. Cr_2O_3 platelets obtained under air are so well crystallized that a punctual SAED pattern could be recorded and indexed successfully along the c^* axis (inset Fig. 4c, index 2). This result is somewhat consistent with the oxidative power of the gases ($N_2 < Ar < R$): The more the gas is oxidizing, the easier the creation of Cr^{3+} will be, and the higher the size and crystallinity of the Cr_2O_3 particles will be. On the opposite, crystallinity and size of the spinel manganese ferri-chromite particles were shown to be non-sensitive to the oxidative power of the used gases. High resolution images as well as corresponding FFT recorded on such highly crystallized particles are reported in Fig. 4, index 3.

We also scrutinized the composition of octahedral-type particles having the spinel structure, and showed that the composition seems to be affected by the various high temperature treatments,

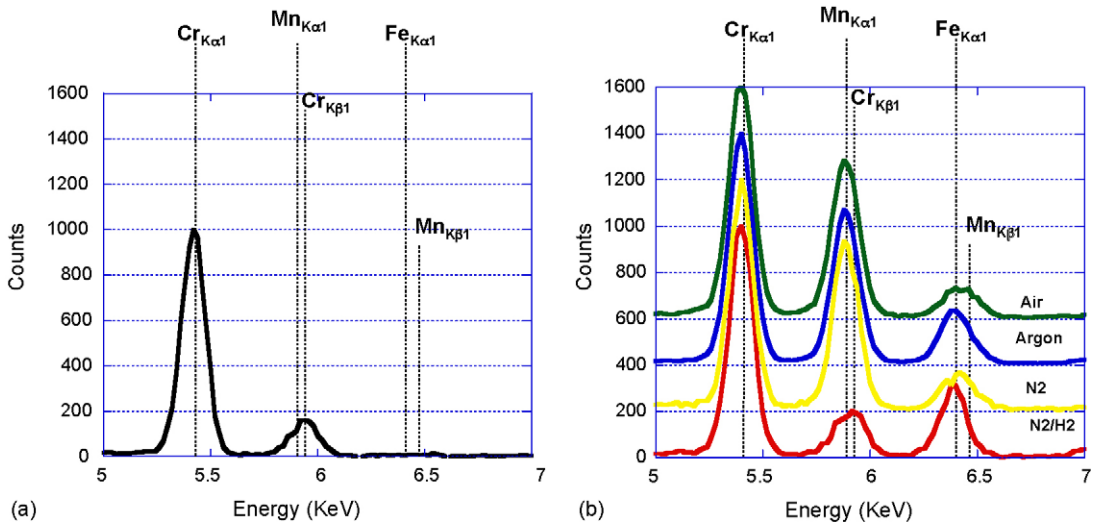

Fig. 5. (a) EDS spectrum recorded on a platelet of the sample treated under N_2/H_2. (b) Comparison of the EDS spectrums recorded on octahedra of the samples treated under N_2/H_2, nitrogen, argon and air.

namely by the nature of the flowing gases. Therefore, it should be recognized that determining quantitatively the Mn, Cr and Fe contents coexisting in a same sample is far from being straightforward with EDS analysis. The reason being that the positions in energy of the theoretical lines for chromium, iron and manganese, as reported in Fig. 5, show a strong overlapping of the Mn $K_\alpha 1$ and Cr $K_\beta 1$ peaks as well as Fe $K_\alpha 1$ and Mn $K_\beta 1$ peaks. A simple solution to bypass this experimental problem consists in monitoring the ratio between the Cr K_α line located at the 5.411 keV and Cr K_β lines located at 5.924 keV. In order to standardize the Cr K_α/Cr K_β ratio, the eskolaite platelets present in all samples, as previously discussed, were used as a reference (Fig. 5a). With such standardization, the presence of manganese in spinel phase could be detected by examining the exact position of the peak around 5.9 eV as well as the evolution of the intensity of this peak.

Fig. 5b shows typical EDS spectra recorded on octahedron-shaped particles from samples treated under N_2/H_2, N_2, Argon or air. The EDS spectrum recorded on the N_2/H_2 sample presents a peak centred on the exact position of the Cr K_β line (the Cr K_α/Cr K_β ratio is in good agreement with the one measured for pure Cr_2O_3) together with an additional peak at 6.4 eV centred on the Fe K_α line. This clearly shows that the spinel phase obtained under N_2/H_2 is manganese-free with an average composition $Fe_{0.7(4)}Cr_{2.3(4)}O_4$. On the opposite, for all the other spectra a shift of the 5.9 eV peak toward lower energy together with an increase in its intensity is noted unambiguously implying the presence of Mn in these samples. This is further confirmed by the appearance of a shoulder on the left side of the 6.4 eV peak that falls perfectly at the energy position of the Mn $K_\beta 1$ peak (6.489 eV). A careful quantification of the manganese/chromium/iron ratios in the N_2, Ar and R samples has led to the following composition $Mn_{1.2(3)}Fe_{0.2(1)}Cr_{1.6(4)}O_4$, $Mn_{1.0(3)}Fe_{0.4(1)}Cr_{1.6(4)}O_4$ and $Mn_{1.1(3)}Fe_{0.2(1)}Cr_{1.7(4)}O_4$ respectively. All of the phase identification and limit composition are summarized in Table 1. From these results, it can be concluded that the presence of hydrogen in the atmosphere seems to prevent manganese from migrating to the surface of the stainless steel pellet.

3.4. Thermal effect

The effect of the temperature on the stainless steel treatment is obvious, by comparing TEM images recorded on the samples treated in air at 700 °C (Fig. 4c) and 800 °C (Fig. 4d). An increase in temperature induces, as expected, an increase in crystallinity and in size of the eskolaite particles. Platelets on the bright field image (Fig. 4d index 1) are pretty large (several microns). The observed marble contrast, well known as Bragg fringes, demonstrates that the crystal is thick and well crystallized. This point is confirmed on both high resolution image (Fig. 4d inset 1) and SAED pattern (inset Fig. 4d inset 2). From the comparison of the SAED patterns recorded on samples treated at 700 and 800 °C, it is worth noting that diffuse grey lines coming from the transmitted beam are spreading towards the diffracted one. This effect, different from the Kikuchi lines effect, is called "the grey background", and is due to inelastic scattering that takes place in thick

Table 1
Summary of the TEM studies showing the composition shape and crystallinity of the observed particles

	Thermal Treatment	Spinel chromite phase	Sesquioxide Eskolaite Cr_2O_3
Increasing oxydative power ↓	700°C H_2/N_2	Platelets $Fe_{0.7(4)}Cr_{2.3(4)}O_4$	Crystallized platelets
	700°C Nitrogen	Octaedra $Mn_{1.2(3)}Fe_{0.2(1)}Cr_{1.6(4)}O_4$	Poorly crystallized platelets
	700°C Argon	Octaedra $Mn_{1.0(3)}Fe_{0.4(1)}Cr_{1.6(4)}O_4$	Badly crystallized platelets
	700°C Air	Octaedra $Mn_{1.1(3)}Fe_{0.2(1)}Cr_{1.7(4)}O_4$	Well crystallized platelets
	800°C Air	Octaedra $Mn_{0.9(3)}Fe_{0.1(1)}Cr_{2.0(4)}O_4$	Large well crystallized platelets

crystals. Overall, we can conclude that the treatment temperature does not affect the shape, size and crystallinity of the octahedral particles, and hardly changes their composition, as deduced from EDS spectrum, which averages around the composition $Mn_{0.9(3)}Fe_{0.1(1)}Cr_{2.0(4)}O_4$ as summarized in Table 1.

3.5. TEM characterization of the cycled nano-structured current collectors

Treated stainless steel disks were investigated for their electrochemical performances at 55 °C versus Li using coin cells hardware [13], but in parallel semi-*ex situ* HRTEM measurements were conducted on reduced samples in order to study whether the mixed ABO_4 oxide, which reacts with lithium according to a conversion process, will give birth to mixed metallic (AB alloy) nanoparticles during discharge or will enlist a segregation mechanism leading to a composite mixture of pure A and B nanograins. To pursue this study, we selected the sample treated under H_2/N_2, which contains spinel phase particles having solely two metal elements (Fe and Cr) as opposed to three (Fe–Cr–Mn) for the other ones, so as to avoid the EDS quantification problems due to Mn–Cr overlapping. We recall that N_2/H_2 treated sample contain pure Cr_2O_3 platelets and $(Fe_xCr_{1-x})(Cr_2)O_4$ with $0.3 < x < 1$ octahedral-type spinel particles. We noted that consequently the composition of the spinel phase differs from one octahedron to another. The experimental protocol for this study is schematized in Fig. 6. The typical voltage-composition curves for such Li/stainless steel treated disks cycled between 0.02 and 3 V at C/5 (insets of Figs. 7 and 8) is at first sight somewhat similar to that obtained for either Li/Cr_2O_3 powder or Li/Cr_2O_3 thin film cells (Fig. 2).

The evolution of both Cr_2O_3 platelets and Fe/Cr-based spinel octahedral particles coexisting within H_2/N_2-treated samples were studied by HRTEM upon its lithiation/delithiation. According to HRTEM investigation (not shown here for conciseness reason), the Cr_2O_3 platelets react versus lithium strictly in the same way as the particles of pure chromium oxide obtained by PLD at 400 °C (as described in the PLD part). Thus, we focussed our attention on the evolution of the spinel octahedral particles after a full discharge and a recharge.

While Bright field image (not shown here) shows that the starting monolithic octahedra transform into nanoparticles agglomerates, the HRTEM images of the fully discharged electrode are reported in Fig. 7 together with the corresponding electronic diffraction pattern. Like for conversion reaction products so far observed, we note the presence of nanoparticles of about 3 nm in size (Fig. 7a). The corresponding SAED pattern (Fig. 7b) reveals the presence of two sets of rings, one corresponding to Li_2O and the other one that could either correspond to metallic Cr or Fe (their electron powder patterns are indiscernible with such a technique). Therefore, owing to the use of nano-probe EDS analysis (Fig. 7c) with a beam that has a diameter (2 nm) smaller than the nanograins size and by selecting nanoparticles on the edge of the agglomerate to avoid interference with others, we could deduce that all of the metal nanoparticles we have investigated (Fig. 7d) within one agglomerate present approximately the same Cr/Fe ratio; so we can confer to the nanoparticles the following composition Fe_xCr_{1-x} $(0.11 \leq x \leq 0.07)$. This result bears some importance as the Fe–Cr phase diagram shows only the composition $Fe_{0.03}Cr_{0.97}$ at 300 °C, thus suggesting that the nanoparticles obtained through a full reduction are thermodynamically metastable.

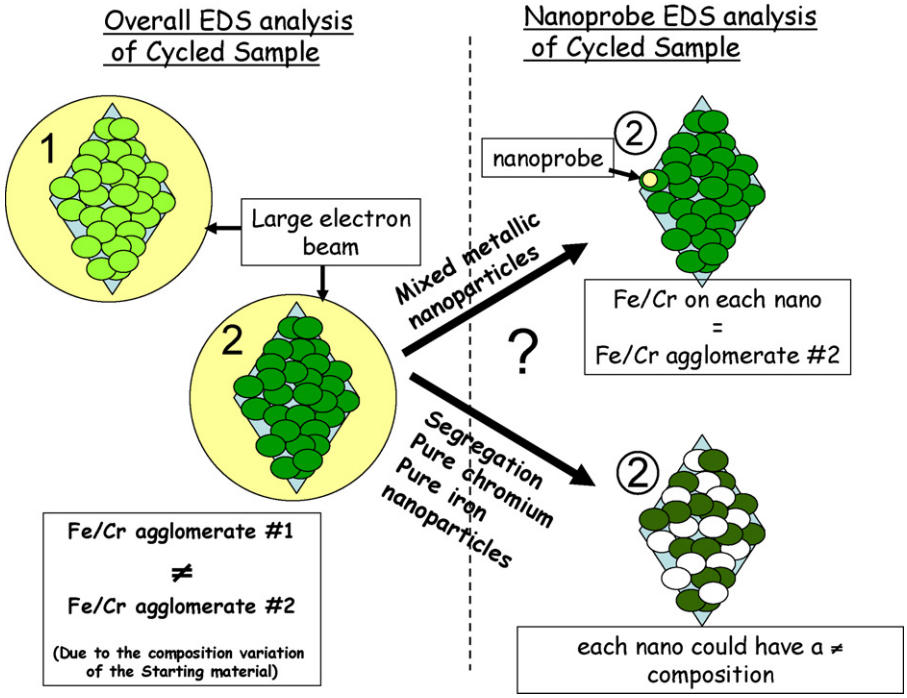

Fig. 6. Scheme showing how nano-probe EDS experiment will allow to distinguish between the formation of mixed Chromium-iron nanoparticles or segregation into pure chromium and pure iron nanoparticles during electrochemical cycling.

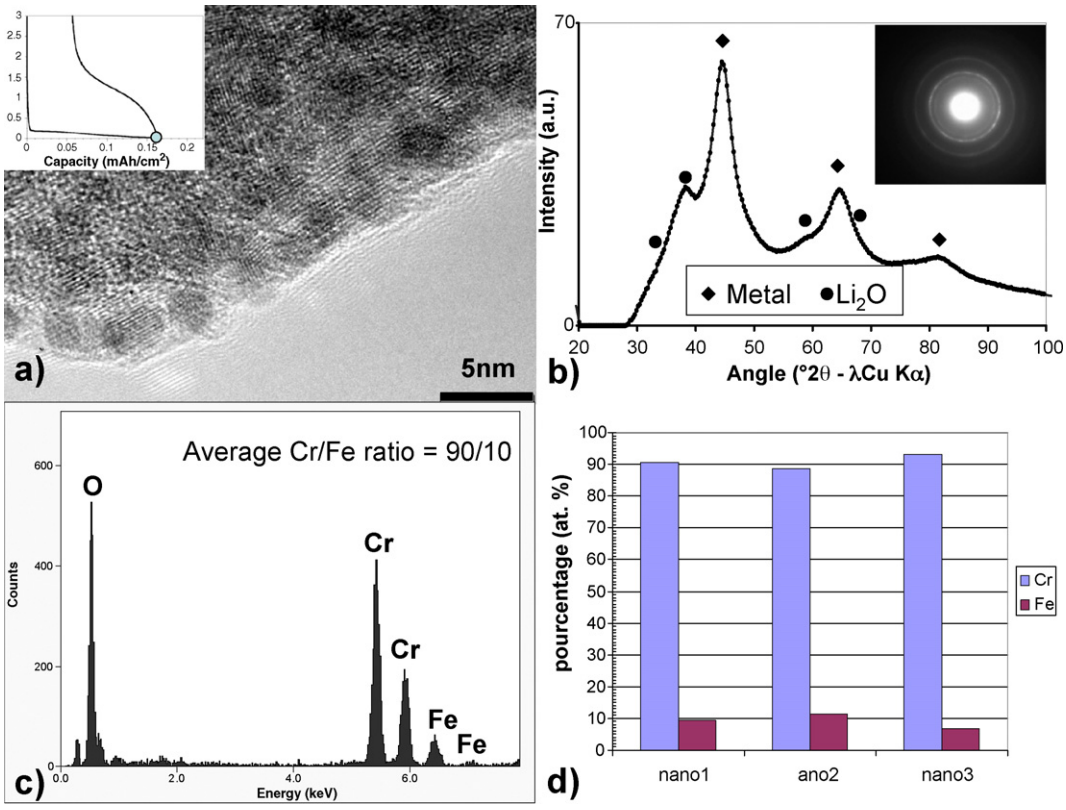

Fig. 7. TEM study realized on treated disks after a full discharge. Typical charge/discharge voltage composition traces for a Li/half-cell is given in inset where the dot denotes the states in which the electrode material was observed by TEM. (a) HRTEM image of the fully discharged electrode showing 3 nm nanoparticles. (b) The corresponding SAED patterns reveal the presence of rings that could correspond either to Cr or Fe + Li_2O. According to nano-beam EDS analysis (d), the nanoparticles contained approximately the same Cr/Fe ratio (90/10) as the one deduced from EDS measurements realized on a larger scale (c).

With such surprising results, it was important to determine the outcome of this iron/chromium alloy during the following charge. Representative HRTEM images together with the corresponding SAED for the fully charged samples are shown Fig. 8. Based on the SAED rings (Fig. 8b), we cannot tell whether the samples contain CrO (JCPDS 78–0722), FeO (JCPDS 75–1550) or a mixed $Fe_xCr_{1-x}O$ phase. Regardless of the determined oxide compositions, we can ascertain that we do not go back to a spinel-type phase, but more simply to an oxide phase containing divalent metal cations, as previously observed with Cr_2O_3 and in agreement with the large irreversibility observed during the first electrochemical cycle versus Li. To solve the dilemma between phase segregation (CrO and FeO) and a solid solution $Fe_xCr_{1-x}O$, we performed a nano-beam EDS analysis (Fig. 8c), in the same conditions as reported above, on several nanoparticles from the same agglomerate (Fig. 8a) and repeated the experiment on several agglomerates. The reader should keep in mind that this study is a semi-*in situ* study, and that the composition of the starting octahedral sample was not homogeneous. Consequently, strong composition variations were reported from one agglomerate to another (in the same or different electrochemical states (discharge/charge)). Nevertheless, the fact that all of the nanoparticles within a given agglomerate have the same Cr/Fe ratio (Fig. 8d) strongly indicates that we most likely dealt with a mixed oxide (as reported on the scheme in Fig. 6). We chose to report the EDS result obtained on one of these agglomerates (Fig. 8d) giving the composition $Fe_{0.35}Cr_{0.65}O$.

This is a quite an interesting finding since we obtained, for the first time to our knowledge, direct evidence of the formation of bimetallic alloy nanoparticles during the Li-driven electrochemical reduction of a mixed transition metal oxide spinel that produces a nano mixed transition metal monoxide upon subsequent oxidation. Strictly speaking, due to the resolution of the EDS probe (20 Å), a segregation of chromium and iron could be imagined at a lower scale with the formation of pure 10 Å CrO and FeO domains. Such a segregation is quite unlikely owing to the fact that the analyzed volume contains only 50 monoxide cells ($a = 4.3$ Å). Nevertheless, previous studies based on ^{57}Fe Mössbauer experiments realized on other full reduced/oxidized mixed oxides, such as $NiFe_2O_4$, have reported the segregation of metals during lithiation and not of a bimetallic alloy [15]. This difference is somewhat surprising since, according to binary phase diagrams, both (Cr, Fe) and (Ni, Fe) systems shows the existence of some solid solutions. While in the case of the chromite-type phases, we identified only monoxides (M^{2+}) from electron diffraction study on the re-oxidized materials, Tirado et al. have shown that a $NiFe_2O_4$ electrode charged to 3 V is made of NiO and Fe_2O_3. Based on our own experience, even with pure Fe_2O_3 powdered samples, we could never succeed in returning to the precursor oxide. As whether such a difference is nested in the sample elaboration or the cycling parameters

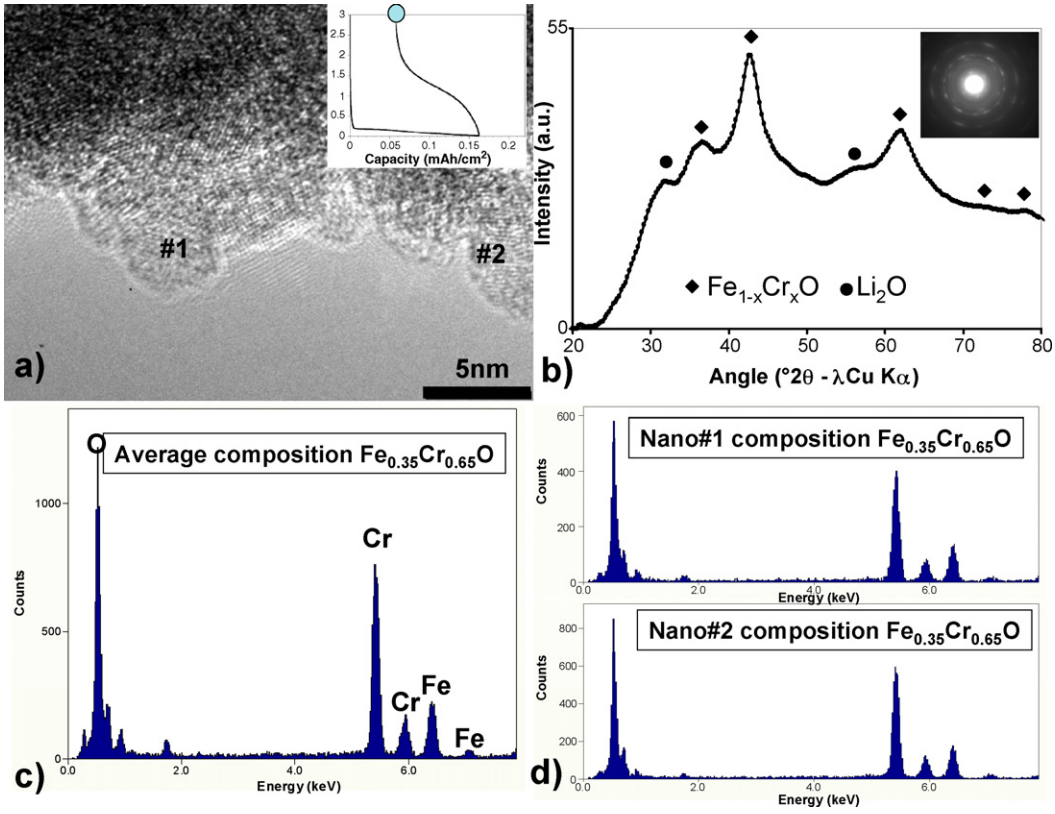

Fig. 8. TEM study realized on treated disks after a full charge. Typical charge/discharge voltage composition traces for a Li/half-cell is given in inset where the dot denotes the states in which the electrode material was observed by TEM. (a) HRTEM images of the fully charged electrode showing 3 nm nanoparticles. (b) The corresponding SAED patterns reveal the presence of remaining Li_2O as well as a CrO-type phase. (c) Average EDS analysis realized on the studied agglomerate. (d) Nano-beam EDS analysis on two different nanoparticles from the same agglomerate showing a composition close to the measured average composition.

(namely cycling rate and electrode preparation) remains an open question that needs to be answered.

4. Conclusions

We have reported, through HTREM studies, the nature of the oxide phases forming other phases during the treatment of stainless steel under various atmospheres and temperatures together with their evolution upon Li electrochemical reduction and oxidation. By finely tuning synthesis condition parameters, we succeeded in tailoring the size, shape, crystallinity and composition of the oxide particles forming the self-supported stainless steel oxide film with namely the absence of Mn in the oxide surface layer for the N_2/H_2 treated samples. Furthermore, we have shown that analytical TEM can be a powerful tool to finely characterize nano-composite samples, and therefore to spot, for the first time, the formation of metastable chromium-iron alloys nano particles rather than metal segregation, during the electrochemical reduction of a mixed binary precursor oxide upon electrochemical reduction by Li. In light of such findings, experiments are being conducted aiming towards: (1) weighing the positive attributes of having a binary Fe–Cr alloy rather than an intimately nano-composite made of Cr and Fe metallic particles on conversion reactions in terms of electrochemical performances and (2) seeking other binary oxides having a similar behaviour as the Fe–Cr ones described here.

Acknowledgments

The authors are indebted to B. Ytriex for sharing with us his long-lasting experience in stainless steel as well as S. Lascaud, E. Vidal and M. Armand for enlightening discussions.

References

[1] B. Scrosati, Challenge of portable power, Nature 373 (1995) 557–558.
[2] J.-M. Tarascon, M. Armand, Issues and challenges facing rechargeable batteries, Nature 414 (2001) 359–367.
[3] W. Waklhara, O. Yamamoto (Eds.), Advances in Lithium-ion Batteries, Kodansha–Wiley–VCH, Wenheim, 1998.
[4] P. Poizot, S. Laruelle, S. Grugeon, L. Dupont, J.-M. Tarascon, Nature (London) 407 (2000) 496.
[5] R. Dedryvère, S. Laruelle, S. Grugeon, P. Poizot, D. Gonbeau, J.-M. Tarascon, Chem. Mater. 16 (2004) 1056.
[6] P. Poizot, S. Laruelle, S. Grugeon, J.-M. Tarascon, J. Electrochem. Soc. 149 (2002) A1212.
[7] S. Laruelle, S. Grugeon, P. Poizot, M. Dollé, L. Dupont, J.-M. Tarascon, J. Electrochem. Soc 149 (2002) A627.

[8] S. Grugeon, S. Laruelle, R. Herrera-Urbina, L. Dupont, P. Poizot, J.-M. Tarascon, J. Electrochem. Soc. 148 (2001) A285.
[10] A. Debart, L. Dupont, P. Poizot, J.-B. Leriche, J.-M. Tarascon, J. Electrochem. Soc. 148 (2001) A1266.
[11] P. Poizot, S. Laruelle, S. Grugeon, J.-M. Tarascon, J. Electrochem. Soc. 149 (2002) A1212.
[12] J. Hu, H. Li, X. Huang, Elec. S.S. Lett. 8 (1) (2005) A66.
[13] S. Grugeon, S. Laruelle, L. Dupont, F. Chevallier, P.L. Taberna, P. Simon, L. Gireaud, S. Lascaud, E. Vidal, B. Yrieix, J.-M. Tarascon, Chem. Mater. 17 (20) (2005) 5041–5047.
[14] J.L. Labar, L. Brno, F. Franck, Ciampor (Eds.), Proceedings of the EUREM, vol. 12, 2000, p. 1379.
[15] R. Alcantara, M. Jaraba, P. Lavela, J.L. Tirado, J.C. Jumas, J. Olivier-Fourcade, Electrochem. Commun. 5 (2003) 16–21.